Resumming transverse observables for NNLO+PS matching in GENEVA

Alessandro Gavardi,[1] Rebecca von Kuk,[1] and Matthew A. Lim[2, 3]

[1]*Deutsches Elektronen-Synchrotron DESY, Notkestr. 85, 22607 Hamburg, Germany*
[2]*Department of Physics and Astronomy, University of Sussex, Sussex House, Brighton, BN1 9RH, UK*
[3]*Università degli Studi di Milano-Bicocca & INFN Sezione di Milano-Bicocca, Piazza della Scienza 3, Milano 20126, Italy*

(Dated: May 22, 2025)

We study the use of higher-order resummation for transverse observables to achieve NNLO+PS matching within the GENEVA framework. In particular, we embed q_T resummation for colour-singlet production at N^3LL obtained via soft-collinear effective theory and implemented in the library SCETLIB within GENEVA. We also study for the first time the use of the generalised N-jettiness variable in parton shower matching, and achieve the resummation of the one-jettiness defined with transverse measures up to NLL' accuracy. As a case study, we use these resummed calculations to construct a GENEVA NNLO+PS generator for Higgs boson production in heavy-quark annihilation (with beauty or charm-quarks in the initial state). The use of transverse measures facilitates the matching to showers ordered in transverse momentum, and opens the door to possible future extensions of this approach to the production of colour singlets in association with final-state jets.

I. INTRODUCTION

The success of the experimental programme at the LHC demands theoretical tools at the highest possible accuracy. While fully-differential calculations at fixed-order in perturbation theory have reached N^3LO for simple processes [1–4], state-of-the-art for predictions matched to parton shower generators is currently next-to-next-to-leading order (NNLO+PS). Two main approaches exist to achieve this accuracy [5, 6], while a third, rather different approach, is currently under active development [7, 8].

An interesting question relevant to the construction of NNLO+PS generators concerns the choice of resolution variables, which partition the phase space into jet bins of differing multiplicity and which must be resummed to high logarithmic accuracies. While many choices are in principle possible, the predictions for exclusive observables will depend on said choice, introducing a source of systematic uncertainty. A natural way to gauge the size of this uncertainty would be to compare the predictions of generators constructed using the same method but different variables. In addition, the availability of higher-accuracy parton shower algorithms [9–12] means that one may wish to explore novel variable choices to ensure the preservation of the shower accuracy in matching.

In this work, we implement a new combination of resolution variables in the GENEVA approach. The original formulation of GENEVA [13] used the zero- and one-jettiness [14] to separate the 0/1- and 1/2- jet bins respectively, and indeed many electroweak processes have since been examined in this context [15–21]. The jettiness variable has the advantage of considerable simplicity, admitting a simple factorisation structure in SCET-I which facilitates resummation [22, 23]. However, the fact that the usual definition of the jettiness involves an invariant mass-like measure complicates the matching to commonly employed parton shower algorithms, which tend to

be ordered in transverse momentum. An alternative formulation using the colour-singlet transverse momentum q_T to separate the 0/1-jet bins was studied in ref. [24], with q_T resummation at N^3LL provided by the RADISH formalism [25, 26]. The 1/2-jet separation variable remained, however, the one-jettiness. In ref. [27], a generator for W^+W^- production was constructed using the hardest and second-hardest jet transverse momenta as variables and SCET-based resummation [28, 29]. With these choices, the need for truncated showering techniques [30] in GENEVA was obviated. A summary of the currently available GENEVA implementations is presented in tab. II.

The new class of generators we initiate in this work uses transverse observables to separate all jet bins, as in ref. [27]. As in ref. [24], we use q_T as the primary resolution variable, though exploiting analytic SCET-II resummation provided by SCETLIB [31] rather than the RADISH approach previously taken. As a secondary resolution variable, we choose a generalisation of the one-jettiness which uses a transverse momentum-like measure. Though the definition of this observable was introduced in the original N-jettiness paper over 15 years ago [14], to our knowledge this is the first time that its resummation has been accomplished beyond leading logarithmic order. [1] The observable is interesting not merely because it facilitates matching for colour singlet processes, but because of the promise it holds for achieving NNLO+PS matching for colour-singlet production in association with additional jets. The work we present here takes a very first step in this direction, achieving resummation at NLL'.

As a case study, we consider the production of a Higgs boson through heavy-quark annihilation ($c\bar{c}, b\bar{b} \rightarrow$

---

[1] We note that a similar generalisation of the jettiness has more recently been proposed in ref. [32].

H). The requisite q_T resummation for this process was achieved at N^3LL in ref. [33], and an NNLO+PS generator for the $b\bar{b}H$ process in the 5-flavour scheme was constructed in ref. [34] using the MiNNLOps formalism. As detailed in e.g. ref. [35], measurements of the Higgs boson q_T spectrum could be used in conjunction with precision theory predictions for $b\bar{b}H$ to extract a value for the bottom Yukawa coupling y_b. Generalisations to other colour-singlet processes, though time-consuming, are in principle straightforward.

The rest of this paper is arranged as follows. In section II, we provide a brief recap of the GENEVA method for matching NNLO calculations to parton shower, while section III summarises q_T resummation in SCET. In section IV we briefly review the definition of the generalised jettiness for unacquainted readers, before detailing the resummation of a specific choice of measures at NLL$'$. We present NNLO+PS matched results for $b\bar{b}H$ and $c\bar{c}H$ in section V, before concluding in section VI.

II. THE GENEVA METHOD

The GENEVA method [5, 13] relies on defining infrared (IR) safe events at a specific perturbative order, which are obtained by combining fixed-order and resummed calculations. This is achieved by converting IR-divergent final states with M partons into IR-finite final states with N partonic jets, where $M \geq N$, ensuring that the divergences cancel on an event-by-event basis. The conversion is performed using N-jet resolution variables r_N to define slicing parameters r_N^{cut}, which divide the phase space into

regions with different numbers of resolved emissions: Φ_0 where there is no additional jet, Φ_1 with one jet and Φ_2 with two or more jets in the final state.

To define the GENEVA differential cross sections with zero, one and two jets, we begin by introducing the following short-hand notation

$$\frac{d\sigma^{NLO_0}}{d\Phi_0}(r_0^{\text{cut}}) = B_0(\Phi_0) + V_0(\Phi_0)$$
$$+ \int \frac{d\Phi_1}{d\Phi_0} B_1(\Phi_1)\,\theta(r_0 < r_0^{\text{cut}}), \quad (1)$$

$$\frac{d\sigma^{NLO_1}}{d\Phi_2}(r_1^{\text{cut}}) = B_1(\Phi_1) + V_1(\Phi_1)$$
$$+ \int \frac{d\Phi_2}{d\Phi_1} B_2(\Phi_2)\,\theta(r_1 < r_1^{\text{cut}}), \quad (2)$$

$$\frac{d\sigma^{LO_2}}{d\Phi_2} = B_2(\Phi_2). \quad (3)$$

where B_M and V_M represent the tree-level and one-loop contributions with M partons in the final state, and we defined

$$\frac{d\Phi_{N+1}}{d\Phi_N} = d\Phi_{N+1}\,\delta[\Phi_N - \tilde{\Phi}_N(\Phi_{N+1})] \quad (4)$$

to indicate the integration over the Φ_{N+1} phase space points that are projected on Φ_N by the $\tilde{\Phi}_N$ mapping. Following the method first developed in ref. [27], the differential cross sections with zero, one and two additional jets are then defined as

$$\frac{d\sigma_0^{MC}}{d\Phi_0}(r_0^{\text{cut}}) = \frac{d\sigma^{N^3LL_{r_0}}}{d\Phi_0}(r_0^{\text{cut}}) - \frac{d\sigma^{N^3LL_{r_0}}}{d\Phi_0}(r_0^{\text{cut}})\bigg|_{NLO_0} + \frac{d\sigma^{NLO_0}}{d\Phi_0}(r_0^{\text{cut}}) \quad (5)$$

$$\frac{d\sigma_1^{MC}}{d\Phi_1}(r_1^{\text{cut}}) = \left\{ \left[\frac{d\sigma^{N^3LL_{r_0}}}{d\Phi_0\,dr_0} - \frac{d\sigma^{N^3LL_{r_0}}}{d\Phi_0\,dr_0}\bigg|_{NLO_1} \right] \mathcal{P}_{0\to1}(\Phi_1)\,U_1(\Phi_1, r_1^{\text{cut}}) \right.$$

$$+ \frac{d\sigma^{NLO_1}}{d\Phi_1}(r_1^{\text{cut}}) + \frac{d\sigma^{NLL'_{r_1}}}{d\Phi_1}(r_1^{\text{cut}}) - \frac{d\sigma^{NLL'_{r_1}}}{d\Phi_1}(r_1^{\text{cut}})\bigg|_{NLO_1} \left. \right\} \theta(r_0 > r_0^{\text{cut}})$$

$$+ \frac{d\sigma^{LO_1}_{\text{nonproj}}}{d\Phi_1}\,\theta(r_0 < r_0^{\text{cut}}) \quad (6)$$

$$\frac{d\sigma_{\geq2}^{MC}}{d\Phi_2} = \left\{ \left[\frac{d\sigma^{N^3LL_{r_0}}}{d\Phi_0\,dr_0} - \frac{d\sigma^{N^3LL_{r_0}}}{d\Phi_0\,dr_0}\bigg|_{NLO_1} \right] \mathcal{P}_{0\to1}(\Phi_1)\,U_1'(\Phi_1, r_1)\,\mathcal{P}_{1\to2}(\Phi_2) \right.$$

$$+ \frac{d\sigma^{LO_2}}{d\Phi_2} + \left[\frac{d\sigma^{NLL'_{r_1}}}{d\Phi_1\,dr_1} - \frac{d\sigma^{NLL'_{r_1}}}{d\Phi_1\,dr_1}\bigg|_{LO_2} \right] \mathcal{P}_{1\to2}(\Phi_2) \left. \right\} \theta(r_1 > r_1^{\text{cut}})\,\theta(r_0 > r_0^{\text{cut}})$$

$$+ \frac{d\sigma^{LO_2}_{\text{nonproj}}}{d\Phi_2}\,\theta(r_1 < r_1^{\text{cut}})\,\theta(r_0 > r_0^{\text{cut}}). \quad (7)$$

In the above equations, $d\sigma^{N^3LL_{r_N},NLL'_{r_N}}/d\Phi_N(r_N)$ and $d\sigma^{N^3LL_{r_N},NLL'_{r_N}}/d\Phi_N\,dr_N$ are respectively the cumulant

and spectrum of the r_N N^{3}LL or NLL$'$ resummed cross section and the notation $|_{\text{(N)LO}_M}$ indicates their fixed-order expansion at the (N)LO order of the process with M final-state partons. Furthermore, $U_1(\Phi_1, r_1)$ denotes the NLL r_1 Sudakov form factor, $U_1'(\Phi_1, r_1)$ its derivative with respect to r_1, and the functions $\mathcal{P}_{N\to N+1}(\Phi_{N+1})$ (called splitting functions in the GENEVA literature) are used to spread the resummed $\mathcal{T}_N$ spectrum over the Φ_{N+1} phase space. They are defined such that

$$\int \frac{\mathrm{d}\Phi_{N+1}}{\mathrm{d}\Phi_N \, \mathrm{d}r_N} \, \mathcal{P}_{N\to N+1}(\Phi_{N+1}) = 1. \qquad (8)$$

Finally, the 'nonproj' label is used to indicate the Φ_{N+1} phase space points that do not have a Φ_N projection through the $\tilde{\Phi}_N$ mapping.

The $\tilde{\Phi}_1$ mapping is constructed in such a way that it preserves the value of r_0, i.e.

$$r_0(\tilde{\Phi}_1(\Phi_2)) = r_0(\Phi_2), \qquad (9)$$

which is crucial to ensure that the r_1 resummation does not spoil the resummed r_0 spectrum. Since we use $r_0 = q_T$ in this work, we require a q_T-preserving mapping in our NLO$_1$ calculation. Mappings which satisfy this criterion have been previously used in refs. [13, 24]. In this work, we construct a new hybrid mapping by combining the ISR part of the $\mathcal{T}_0 - q_T$ preserving mapping from ref. [13] with the FSR part of the mapping used in ref. [27] which preserves the transverse momentum of the jet, p_T^{jet}. This has better numerical performance compared to the q_T preserving mapping of ref. [24] while still avoiding unphysical artefacts in exclusive distributions, which are caused by the FSR part of the $\mathcal{T}_0 - q_T$ mapping.

The integration measure introduced in eq. (8) is defined as

$$\begin{aligned}\frac{\mathrm{d}\Phi_{N+1}}{\mathrm{d}\Phi_N \, \mathrm{d}r_N} =&\,\mathrm{d}\Phi_{N+1}\, \delta[\Phi_N - \bar{\Phi}_N(\Phi_{N+1})] \\ &\times \delta[r_N - r_N(\Phi_{N+1})] \qquad (10)\end{aligned}$$

and indicates the integration over the Φ_{N+1} phase space points whose value of the N-jet resolution variable is r_N and which are projected on Φ_N by the $\bar{\Phi}_N$ mapping (called splitting mapping in the GENEVA literature). The $\bar{\Phi}_N$ mapping does not need to coincide with $\tilde{\Phi}_N$. Indeed, to simplify the implementation of the $\mathcal{P}_{1\to 2}$ functions, in this work we employ a splitting mapping $\bar{\Phi}_N \neq \tilde{\Phi}_N$, whose details are discussed in section IV C.

III. RESUMMATION OF TRANSVERSE MOMENTUM IN SCET

The factorisation of the leading-power q_T spectrum was first established in refs. [36–38], and extended in refs. [39–41]. In this paper, we adopt the SCET framework [42–46], where q_T factorisation was formulated in

refs. [47–50]. In particular, we employ rapidity renormalisation [49, 51] using the exponential regulator [50]. In this formulation, the singular cross section for colour-singlet production can be written as

$$\begin{aligned}\frac{\mathrm{d}\sigma^{\text{sing}}}{\mathrm{d}q_T \, \mathrm{d}\Phi_0} =& \sum_{a,b} H_{ab}(\Phi_0; \mu) \int \mathrm{d}^2\vec{k}_a \, \mathrm{d}^2\vec{k}_b \, \mathrm{d}^2\vec{k}_s \qquad (11) \\ &\times \delta(q_T - |\vec{k}_a - \vec{k}_b - \vec{k}_s|) B_a(x_a, \vec{k}_a; \mu, \nu/\omega_a) \\ &\times B_b(x_b, \vec{k}_b; \mu, \nu/\omega_b) \, S_{ab}(\vec{k}_s; \mu, \nu).\end{aligned}$$

The hard function H_{ab} is process-dependent and describes the hard interaction producing the colour singlet $ab \to F$, where a, b denote the available partonic channels at leading order. The beam functions $B_{a,b}$ describe collinear radiation with total transverse momentum $\vec{k}_{a,b}$ and longitudinal momentum fractions $x_{a,b} = (m/E_{\text{cm}})e^{\pm Y}$ (for colour-singlet mass m, rapidity Y and hadronic centre-of-mass energy E_{cm}), with $\omega_{a,b} = x_{a,b}E_{\text{cm}}$. The soft function S_{ab} describes soft radiation with total transverse momentum $\vec{k}_s$. Finally, the scales μ and ν denote the virtuality and rapidity renormalisation scales.

To achieve all-order resummation, each of the functions in eq. (11) is first evaluated at its natural scale(s) $\mu_{H,B,S}$, $\nu_{B,S}$, and then evolved to a common set of scales μ, ν by solving a coupled system of renormalisation group equations. As shown in ref. [52], the exact solution of said equations in q_T space in terms of distributions is equivalent to the canonical solution in b_T space appropriately transformed. In this work we follow common practice and employ the latter solution. For details see refs. [52–54].

While the resummed cross section in eq. (11) is appropriate when describing events at low q_T, for higher values it is no longer adequate and we must rely on a calculation at fixed order in perturbation theory. The matching of resummed and fixed order calculations is achieved additively as detailed in sec. II – we are still required, however, to specify a prescription which switches off the resummation at large q_T to ensure a smooth transition between the resummed and fixed-order parts of the calculation. This is achieved using hybrid profile scales [55–57], which allow μ_H, μ_B, μ_S to take different values in the resummation region (required to minimise the size of large logarithms), but which flow to a common scale with increasing q_T, thus naturally ending RG evolution for $q_T \sim Q$.

The framework described above is sufficiently general to describe the production of any colour-singlet final state (given an appropriate hard function). However, implementation details are in general process-dependent. In particular, the shape of the profile scales which determine the transition between resummation and fixed-order regions of phase space is normally chosen based on the relative size of the singular and nonsingular contributions as a function of q_T and differs between e.g. Drell-Yan and Higgs boson production. In our specific case of Higgs boson production in heavy-quark annihilation, these con-

siderations were examined in ref. [33]. Since we directly interface the SCETlib q_T module [58] used in that work to GENEVA, we employ the same central scale choices and profile shapes as used there. We also estimate our uncertainties via profile scale variation in the same manner. We note that just as in ref. [21], this allows us to separate dependence on the beam and factorisation scales μ_B and μ_F, allowing us to perform 7-point scale variations for inclusive observables. For the sake of completeness, we detail our profile scale choices, transition points and variation prescription in app. A.

IV. RESUMMATION OF ONE-JETTINESS WITH GENERALISED MEASURES

A. Observable definition

The N-jettiness observable is most often defined as

$$\mathcal{T}_N = \sum_i \min_m \left\{ \frac{2q_m \cdot p_i}{Q_m} \right\}, \qquad (12)$$

where the sum runs over the four-momenta of all coloured particles p_i^μ, the minimisation over m runs over all beam and jet reference momenta q_m^μ, and the factors Q_m are normalisation factors. This definition uses an invariant mass-like measure and obeys a SCET-I type factorisation, which has been well-studied in the literature.

It was remarked in the original N-jettiness paper, however, that the definition in eq. (12) can be extended to use generic measures in each beam or jet region [14]. Moreover, N-jettiness can be thought of not merely as an event-shape, but as a way to define an exclusive jet algorithm which partitions the phase space into two beam and N jet regions, to which emissions are assigned. The measure factors which are used to assign emissions to each region need not be identical to the value which the observable returns. In general, therefore, we must define separate distance measures $d_m(p_i)$ which assign the emission i to one of the $N + 2$ regions m if

$$d_m(p_i) = \min \left\{ d_1(p_i), \ldots, d_N(p_i), d_a(p_i), d_b(p_i) \right\}, \quad (13)$$

and the resulting observable f_m which is returned by that emission once it falls into the region m,

$$\mathcal{T}^{(m)} = \sum_{i \in m} f_m(\eta_i, \phi_i) p_{T,i}, \qquad (14)$$

where η_i, ϕ_i and $p_{T,i}$ denote the pseudorapidity, azimuth and transverse momentum associated with i. We remark that the definitions of the jet regions d_j for $j \in \{1, \ldots, N\}$ are themselves dependent on a determination of the jet axes, which may be performed either by running an exclusive jet algorithm (e.g. anti-k_T) over the final state, or by a minimisation of the N-jettiness over all possible axes. The latter definition has the advantage of guaranteeing insensitivity to soft-recoil effects, whose correct

treatment requires the introduction of additional transverse momentum convolutions in the factorisation formula. At one-loop, it is equivalent to using the winnertake-all (WTA) axis [59], in that the jet direction is determined solely by the 'hardest' emission.

This generalised definition of the N-jettiness has also been well-studied in the literature, and the choice of the measures has important consequences for the structure of the factorisation. The XCone algorithm implements precisely the procedure described above to act as an exclusive jet algorithm, and in that context a number of different measure choices have been studied [60]. ref. [61] completed the study of factorisation types (i.e., all possible combinations of SCET-I/SCET-II measures for beams and jets) and provided the one-loop soft functions relevant for colour singlet production in association with a single jet. In addition, the N-subjettiness observable, introduced in ref. [62] as a way to study jet substructure, uses choices of the f_m which are transverse momentum-like by default.

In this work, we will make specific choices for both the d_m and f_m and use $N = 1$, thus defining a generalised one-jettiness observable which we refer to as $\mathcal{T}_1^{p_T}$. Specifically, we choose the conical measure [60, 63] for the region assignment, which (for isolated jets) clusters in a manner equivalent to the anti-k_T algorithm:

$$d_0(p_i) = 1, \qquad d_{m \geq 1}(p_i) = \frac{R_{im}^2}{R^2}. \qquad (15)$$

In the above equation, we have defined a single beam measure,

$$d_0(p_i) = \min\{d_a(p_i), d_b(p_i)\}, \qquad (16)$$

and introduced the distance

$$R_{im} \equiv \sqrt{(\eta_i - \eta_m)^2 + (\phi_i - \phi_m)^2} \qquad (17)$$

and (constant) jet radius R. For the measurement itself, defining

$$\mathcal{T}_1^{p_T} = \sum_i \begin{cases} p_{T,i}\, f_B(\eta_i), & \text{for } d_B(p_i) < d_J(p_i), \\ p_{T,i}\, f_J(\eta_i, \phi_i), & \text{for } d_J(p_i) < d_B(p_i), \end{cases} \qquad (18)$$

we choose the boost-invariant generalisation of broadening [61, 64] for the jet region,

$$\begin{aligned} f_J(\eta_i, \phi_i) &= \sqrt{2\cosh(\eta_i - \eta_J) - 2\cos(\phi_i - \phi_J)} \\ &\equiv \mathcal{R}_{iJ} \end{aligned} \qquad (19)$$

where the distance is measured with respect to the jet axis J, and the transverse energy for the beam region,

$$f_B(\eta_i) = 1. \qquad (20)$$

Both observables are of SCET-II type – the setup described above corresponds to one of the choices made in

ref. [61], for which the one-loop soft function was calculated. It was shown in that work that the cross section then factorises as

$$
\frac{d\sigma_\kappa}{d\Phi_1 \, d\mathcal{T}_1^{p_T}} = H_\kappa(\Phi_1, \mu) \int \left(\prod_n dk_n \right)
$$

$$
\times S_\kappa \left(\mathcal{T}_1^{p_T} - \sum_i k_i, \{n_m\}, \{d_m\}, \mu, \frac{\nu}{\mu} \right)
$$

$$
\times B_{\kappa_a} \left(k_a, x_a, \mu, \frac{\nu}{\omega_a} \right) B_{\kappa_b} \left(k_b, x_b, \mu, \frac{\nu}{\omega_b} \right)
$$

$$
\times J_{\kappa_j} \left(k_j, \mu, \frac{\nu}{\omega_j} \right) , \tag{21}
$$

where the channel index $\kappa \equiv \{\kappa_a, \kappa_b, \kappa_j\}$ runs over all possible flavours of incoming and outgoing partons.

B. Ingredients and resummation at NLL′

At NLL′ accuracy, each of the hard, soft, beam and jet functions are required at one-loop accuracy as are the noncusp anomalous dimensions, while the cusp anomalous dimension is needed one order higher. The hard function is easily obtained from the corresponding one-loop QCD amplitude.[2] It satisfies an evolution equation

$$
\mu \frac{d}{d\mu} \ln H_\kappa(\Phi_1, \mu) = \gamma_H^\kappa(\Phi_1, \mu) \tag{22}
$$

where the hard anomalous dimension is of the form

$$
\gamma_H^\kappa(\Phi_1, \mu) = \Gamma_{\rm cusp}[\alpha_s(\mu)] \left[\mathbf{T}_a^2 \ln \frac{\omega_a^2 e^{-2\eta_J}}{\mu^2} \right.
$$

$$
\left. + \mathbf{T}_b^2 \ln \frac{\omega_b^2 e^{2\eta_J}}{\mu^2} + \mathbf{T}_j^2 \ln \frac{\omega_j^2}{(2\cosh\eta_J)^2 \mu^2} \right]
$$

$$
+ \gamma_H^\kappa[\alpha_s(\mu)] , \tag{23}
$$

$$
\gamma_H^\kappa[\alpha_s(\mu)] = (n_q + n_{\bar{q}})\gamma^q[\alpha_s(\mu)] + n_g \gamma^g[\alpha_s(\mu)] , \tag{24}
$$

where n_q and n_g label respectively the number of quarks and gluons in the channel κ.

The relevant soft function was calculated in ref. [61]. Its evolution equation reads

$$
\mu \frac{d}{d\mu} S_\kappa \left(k_S, \Phi_1, \mu, \frac{\nu}{\mu} \right) =
$$

$$
\int dk_S' \gamma_{\mu,S}^\kappa \left(k_S - k_S', \Phi_1, \mu, \frac{\nu}{\mu} \right) S_\kappa \left(k_S', \Phi_1, \mu, \frac{\nu}{\mu} \right) \tag{25}
$$

where we have suppressed the dependence on the d_m for brevity and translated the dependence on the reference

___

[2] Although in general both hard and soft functions are matrices in colour space, for the case of $N = 1$ the colour algebra diagonalises and it is possible to rewrite the factorisation in the form eq. (21).

directions n_m into a dependence on the phase space Φ_1. The soft virtuality anomalous dimension is given to all orders by

$$
\gamma_{\mu,S}^\kappa \left(k_S, \Phi_1, \mu, \frac{\nu}{\mu} \right) = 2\Gamma_{\rm cusp}[\alpha_s(\mu)] \, \delta(k_S)
$$

$$
\times \left[- \left(\mathbf{T}_a^2 + \mathbf{T}_b^2 + \mathbf{T}_j^2 \right) \ln \frac{\nu}{\mu} \right.
$$

$$
+ \mathbf{T}_j^2 \ln(2\cosh\eta_J) + (\mathbf{T}_a^2 - \mathbf{T}_b^2)\eta_J \bigg]
$$

$$
+ \gamma_{\mu,S}^\kappa[\alpha_s(\mu)] \, \delta(k_S) \tag{26}
$$

where the noncusp term $\gamma_{\mu,S}^{\kappa\,(0)}[\alpha_s(\mu)] = 0$ at one-loop. The soft function also obeys a rapidity evolution equation

$$
\nu \frac{d}{d\nu} S_\kappa \left(k_S, \Phi_1, \mu, \frac{\nu}{\mu} \right) =
$$

$$
\int dk_S' \gamma_{\nu,S}^\kappa (k_S - k_S', \mu) \, S_\kappa \left(k_S', \Phi_1, \mu, \frac{\nu}{\mu} \right) \tag{27}
$$

where the rapidity anomalous dimension at one-loop order is given by

$$
\gamma_{\nu,S}^{\kappa\,(1)}(k_S, \mu) = 2\Gamma_0 \frac{\alpha_s(\mu)}{4\pi} \left[\left(\mathbf{T}_a^2 + \mathbf{T}_b^2 + \mathbf{T}_j^2 \right) \frac{1}{\mu} \mathcal{L}_0 \left(\frac{k_S}{\mu} \right) \right] \tag{28}
$$

and the plus distribution $\mathcal{L}_0(x)$ is defined as in app. B.

The collinear beam functions relevant for the observable are those calculated at one-loop in e.g. refs. [28, 65, 66] while the recoil-free broadening jet function was calculated in ref. [59]. Both beam and jet functions obey a set of similar evolution equations,

$$
\mu \frac{d}{d\mu} B_i \left(k_B, x, \mu, \frac{\nu}{\omega} \right) =
$$

$$
\int dk_B' \gamma_{\mu,B}^i \left(k_B - k_B', \mu, \frac{\nu}{\omega} \right) B_i \left(k_B', x, \mu, \frac{\nu}{\omega} \right) , \tag{29}
$$

$$
\nu \frac{d}{d\nu} B_i \left(k_B, x, \mu, \frac{\nu}{\omega} \right) =
$$

$$
\int dk_B' \gamma_{\nu,B}^i (k_B - k_B', \mu) \, B_i \left(k_B', x, \mu, \frac{\nu}{\omega} \right) , \tag{30}
$$

$$
\mu \frac{d}{d\mu} J_i \left(k_J, \mu, \frac{\nu}{\omega} \right) =
$$

$$
\int dk_J' \gamma_{\mu,J}^i \left(k_J - k_J', \mu, \frac{\nu}{\omega} \right) J_i \left(k_J', \mu, \frac{\nu}{\omega} \right) , \tag{31}
$$

$$
\nu \frac{d}{d\nu} J_i \left(k_J, \mu, \frac{\nu}{\omega} \right) =
$$

$$
\int dk_J' \gamma_{\nu,J}^i (k_J - k_J', \mu) \, J_i \left(k_J', \mu, \frac{\nu}{\omega} \right) , \tag{32}
$$

where the virtuality anomalous dimensions take the

forms

$$\gamma^i_{\mu,B}\left(k_B,\mu,\frac{\nu}{\omega}\right) = \left\{2\mathbf{T}_i^2\Gamma_{\mathrm{cusp}}\log\frac{\nu}{\omega} + \gamma^i_B[\alpha_s(\mu)]\right\}\delta(k_B),$$

$$\tag{33}$$

$$\gamma^i_{\mu,J}\left(k_J,\mu,\frac{\nu}{\omega}\right) = \left\{2\mathbf{T}_i^2\Gamma_{\mathrm{cusp}}\log\frac{\nu}{\omega} + \gamma^i_J[\alpha_s(\mu)]\right\}\delta(k_J),$$

$$\tag{34}$$

and at one loop $\gamma^{i\,(0)}_{B/J}[\alpha_s(\mu)] = -2\gamma^{i\,(1)}[\alpha_s(\mu)]$. The one-

loop rapidity anomalous dimensions are instead given by

$$\gamma^i_{\nu,B}(k_B,\mu) = -2\Gamma_0\frac{\alpha_s(\mu)}{4\pi}\mathbf{T}_i^2\frac{1}{\mu}\mathcal{L}_0\left(\frac{k_B}{\mu}\right)\tag{35}$$

$$\gamma^i_{\nu,J}(k_J,\mu) = -2\Gamma_0\frac{\alpha_s(\mu)}{4\pi}\mathbf{T}_i^2\frac{1}{\mu}\mathcal{L}_0\left(\frac{k_J}{\mu}\right).\tag{36}$$

The evolution equations in μ and ν are most easily solved by transforming to Laplace space, first evolving from $\nu_X \to \nu$ at fixed μ_X and subsequently from $\mu_X \to \mu$ (for $X \in \{B,S,J\}$). At NLL, the solution for the soft function can be written analytically as

$$S_\kappa\left(k_S,\Phi_1,\mu,\frac{\nu}{\mu}\right) =$$

$$\exp\left\{2(C_{\kappa_a}+C_{\kappa_b}+C_{\kappa_j})K_\Gamma(\mu_S,\mu) + \left[2(C_{\kappa_a}-C_{\kappa_b})\eta_J + 2C_{\kappa_j}\ln(2\cosh\eta_J) + 2(C_{\kappa_a}+C_{\kappa_b}+C_{\kappa_j})\ln\frac{\mu_S}{\nu}\right]\eta_\Gamma(\mu_S,\mu)\right\}$$

$$\times \int \mathrm{d}k'_S \mathcal{V}_{\eta^\kappa_S}(k_S - k'_S,\mu_S)\, S_\kappa\left(k'_S,\Phi_1,\mu_S,\frac{\nu_S}{\mu_S}\right),\tag{37}$$

$$\eta^\kappa_S = \frac{\alpha_s(\mu_S)}{4\pi}2\Gamma_0\left(C_{\kappa_a}+C_{\kappa_b}+C_{\kappa_j}\right)\ln\left(\frac{\nu}{\nu_S}\right),\tag{38}$$

where the function $\mathcal{V}_a(k,\mu)$ is defined in app. B and the quadratic Casimir factors $C_i = \mathbf{T}_i^2$. Similarly, the solution for the beam and jet functions can be written as

$$B_i\left(k_B,x,\mu,\frac{\nu}{\omega}\right) =$$

$$\exp\left\{K_\gamma(\mu_B,\mu) + 2C_i\ln\frac{\nu}{\omega}\eta_\Gamma(\mu_B,\mu)\right\}\int \mathrm{d}k'_B \mathcal{V}_{\eta^i_B}(k_B - k'_B,\mu_B)\, B_i\left(k'_B,x,\mu_B,\frac{\nu_B}{\mu_B}\right),\tag{39}$$

$$\eta^i_B = -\frac{\alpha_s(\mu_B)}{4\pi}2\Gamma_0\,C_i\ln\left(\frac{\nu}{\nu_B}\right),\tag{40}$$

$$J_i\left(k_J,\mu,\frac{\nu}{\omega}\right) =$$

$$\exp\left\{K_\gamma(\mu_J,\mu) + 2C_i\ln\frac{\nu}{\omega}\eta_\Gamma(\mu_J,\mu)\right\}\int \mathrm{d}k'_J \mathcal{V}_{\eta^i_J}(k_J - k'_J,\mu_J)\, J_i\left(k'_J,\mu_J,\frac{\nu_J}{\mu_J}\right),\tag{41}$$

$$\eta^i_J = -\frac{\alpha_s(\mu_J)}{4\pi}2\Gamma_0\,C_i\ln\left(\frac{\nu}{\nu_J}\right).\tag{42}$$

$\sigma^{\mathrm{NNLO}}_{b\bar{b}\to H}$ [fb]	SusHi	$q_T^{\mathrm{cut}} = 1\,\mathrm{GeV}$	$q_T^{\mathrm{cut}} = 5\,\mathrm{GeV}$	$q_T^{\mathrm{cut}} = 10\,\mathrm{GeV}$
$\mu = m_H$	543.5 ± 0.5	544.3 ± 1.0	544.9 ± 0.8	548.6 ± 0.4
$\mu = m_H/2$	518.0 ± 0.5	518.5 ± 1.1	517.8 ± 0.8	518.4 ± 0.5
$\mu = 2m_H$	581.7 ± 0.6	583.3 ± 0.9	585.1 ± 0.7	591.4 ± 0.4

TABLE I: Comparison between SUSHI and GENEVA of predictions for the NNLO total cross section in $b\bar{b} \to H$. GENEVA predictions at various values of q_T^{cut} are shown, and at various values of $\mu = \mu_R = \mu_F$.

For convenience, we reproduce the one-loop expressions for soft, beam and jet functions in app. C. We note that

while it is possible to write down the solutions of the evolution equations analytically at NLL (NLL$'$) order, extending the above solutions to higher resummed orders seems challenging. The underlying reason for this is a combination of the facts that the evolution equations are solved in Laplace space and that the rapidity anomalous dimensions have a non-trivial dependence on $k_{B,S,J}$. At one-loop order, this necessitates taking an inverse Laplace transform of functions of the form $\exp(-a \ln x)$, for constant a. While this is still possible analytically at this order, the appearance of higher powers of the logarithm in the exponent (arising ultimately from higher plus distributions $\mathcal{L}_{1,2,\dots}$ in γ_ν) hinders an analytic treatment starting at NNLL. Resummation at this order is therefore likely to require a numerical implementation of the inverse integral transform, as is normally performed for q_T resummation.

C. Splitting mappings

To generate events that are distributed according to the NLL$'$ $\mathcal{T}_1^{p_T}$ resummed spectrum, GENEVA assigns the events a weight obtained by multiplying the spectrum by a function (called splitting function in the GENEVA literature) of the $d\Phi_2$ phase space that integrates to 1 for every underlying Φ_1 phase space point and $\mathcal{T}_1^{p_T}$ value:

$$\int \frac{d\Phi_2}{d\Phi_1\, d\mathcal{T}_1^{p_T}}\, \mathcal{P}_{1\to 2}\,(\Phi_2) = 1. \qquad (43)$$

The details of the numeric implementation and the functional forms of the splitting functions used by GENEVA are provided in refs. [21, 67].

This procedure requires introducing a projection $\bar{\Phi}_1$ (called a splitting mapping in the GENEVA literature) from the phase space $d\Phi_2$ to the underlying phase space $d\Phi_1$. The choice of such a projection is constrained by the requirement of infrared safety that univocally fixes the splitting mapping in the limit of small $\mathcal{T}_1^{p_T}$. At large $\mathcal{T}_1^{p_T}$, instead, the choice is largely arbitrary, to the point that not all the phase space points are even required to be projectable (a non-projectable Φ_2 phase space point would simply imply that $P_{1\to 2}(\Phi_2) = 0$). The arbitrariness of this choice might appear to translate into a large theoretical uncertainty in the final distributions. This, however, is not the case, since the splitting functions always multiply differences between resummed spectra and their truncated perturbative expansion, which, at large values of $\mathcal{T}_1^{p_T}$, are beyond the accuracy of the calculation. In other words, different choices of splitting mappings introduce distortions in the distributions of the generated events, whose size is formally subleading with respect to the claimed NNLO accuracy.

For some distributions of particular importance, however, it might be preferable to avoid these kinds of effects entirely. To that purpose, we can exploit the freedom in the choice of the mapping to enforce the preservation of a set of observables O_i, for which

$$O_i(\Phi_2) = O_i\big(\bar{\Phi}_1(\Phi_2)\big). \qquad (44)$$

For these observables, the $\mathcal{T}_1^{p_T}$ resummation can be implemented in a unitary fashion, such that their distributions remain unaffected.

In this work, we require the splitting mapping to preserve the entire colour singlet four-momentum. This guarantees that the NNLO accuracy of the Higgs rapidity distribution and the N^{3}LL$'$ accuracy of the Higgs transverse momentum distribution are not spoiled. This condition still leaves one degree of freedom that we fix with the further constraint that the splitting mapping also preserves the rapidity of the 'hardest' final-state parton (i.e., the one that defines the jet direction in the WTA clustering). The choice of $\mathcal{T}_1^{p_T}$ as 1-jet resolution variable does not constrain the mapping, but affects the numeric implementation of the splitting functions. Guaranteeing that eq. (44) is satisfied indeed requires an analytic computation of the integration limits on Φ_2 at fixed $\Phi_1 = \bar{\Phi}_1(\Phi_2)$ and $\mathcal{T}_1^{p_T}$, as well as the measure $d\Phi_2/d\Phi_1\, d\mathcal{T}_1^{p_T}$.

V. RESULTS

In this section, we present our numerical results for the $q\bar{q} \to H$ process in a proton-proton scattering. We use the following input parameters: $E_{\rm cm} = 13\,{\rm TeV}$, Higgs boson mass $m_H = 125\,{\rm GeV}$ and strong coupling $\alpha_s(m_Z) = 0.118$ with $m_Z = 91.1876\,{\rm GeV}$. Unless otherwise indicated we use the `MSHT20nnlo` PDF set [68]. The Yukawa couplings are computed by evolving the $\overline{\rm MS}$ quark masses $\overline{m}_q(m_q)$ to the desired scale. The input values are $\overline{m}_b(\overline{m}_b) = 4.18\,{\rm GeV}$ and $\overline{m}_c(\overline{m}_c) = 1.27\,{\rm GeV}$ [69]. Finally, we set the Higgs vacuum expectation value to $v = 246.22\,{\rm GeV}$.

A. Fixed order validation

We begin by validating our results at fixed order in perturbation theory. Before presenting our numerical comparisons, we take this opportunity to remind the reader of a subtlety in choosing the renormalisation scale in a resummed calculation, which will affect our results. The profile scales which we employ in GENEVA are functions of the resolution variable q_T. The consequence of this is that the operations of setting the scale and integrating the q_T spectrum to obtain the total cross section (or an inclusive distribution such as the colour singlet rapidity) do not commute. This leaves some freedom in how we present our results – we can either set scales in the spectrum and obtain inclusive quantities by integration, or instead set scales in the integrated cross section and obtain the spectrum by differentiation. The two options differ by formally higher-order terms, which however can
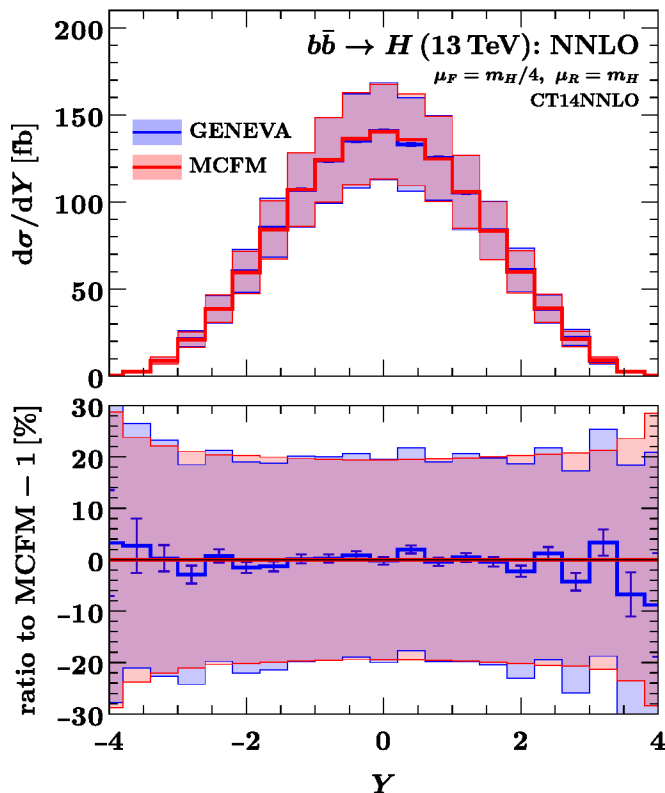
FIG. 1: Comparison between MCFM and GENEVA for the NNLO Higgs boson rapidity spectrum in $b\bar{b} \to H$. Uncertainty bands are obtained via a 7-pt. scale variation procedure.

FIG. 2: Comparison between SCETLIB and GENEVA for the N³LL Higgs boson q_T spectrum in $b\bar{b} \to H$. Uncertainty bands are obtained as explained in app. A

be numerically sizeable. The first choice is more natural when one is interested in the q_T spectrum, since it matches what one would normally do in a resummed calculation. The latter instead guarantees that the results of a fixed order calculation (say, the NNLO cross section) are recovered, but may result in distortions of the q_T spectrum.

In ref. [13], a compromise was proposed. The key idea is to set scales in the spectrum, but to add back a higher-order term which is given by the difference of the spectrum and the q_T-derivative of the cumulant. This is further modulated by an interpolating function $\kappa(q_T)$, which limits the activity of the term to the small q_T region. In this way, one obtains the correct fixed order normalisation for inclusive quantities while minimising any distortions of the q_T spectrum. In this work, we have chosen not to adopt this approach. For the $b\bar{b} \to H$ process in particular, the difference between spectrum and cumulant scale setting is a numerically large effect (in contrast to e.g. Drell-Yan), and our predictions would be extremely sensitive to the exact way in which the cross section fix was implemented. In the rest of this subsection, we have set scales in the cumulant (which facilitates the comparison of our results with fixed order codes). In following subsections, however (and in particular when examining exclusive distributions such as the q_T spec-
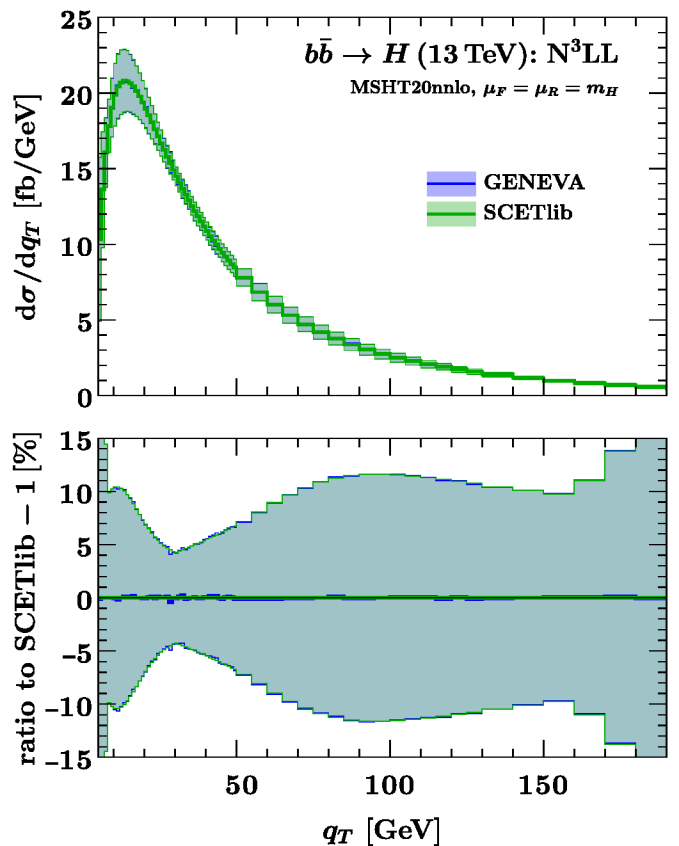
trum), we have instead adopted spectrum scale setting. This is in general more appropriate for Higgs boson production in heavy-quark fusion, since measurements of the Higgs boson q_T spectrum are likely to be one of the few ways in which this process can be probed – spectrum scale setting will therefore lead to the 'best' description for this observable.

The GENEVA predictions for the inclusive cross section at various values of $q_T^{\rm cut}$ are shown in tab. I, and compared to NNLO predictions obtained from SUSHI [70]. The absence of a fully local NNLO subtraction means that the implementation of eq. (5) in GENEVA is done only in an approximate fashion, dropping all fixed order NNLO terms and relying on the singular approximation to the cross section at leading power to provide the two-loop information [13, 15]. This is exactly equivalent to an NNLO calculation in the limit $q_T^{\rm cut} \to 0$; however, for finite values one misses $\mathcal{O}(\alpha_s^2)$ power corrections below $q_T^{\rm cut}$. It is therefore desirable to set the cut as small as possible to minimise the effect of these inclusive nonsingular terms. The differences we observe with respect to the exact calculation implemented in SUSHI are minor, reaching only 1% even at very large values $q_T^{\rm cut} = 10$ GeV: moreover, for $q_T^{\rm cut} = 1$ GeV the GENEVA cross section is equivalent to that returned by SUSHI to within the statistical pre-
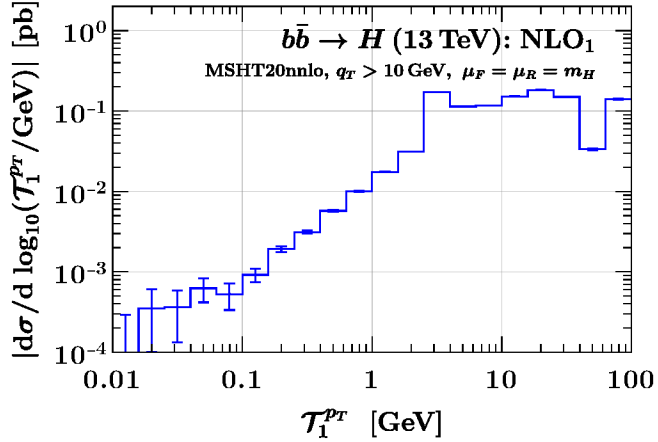
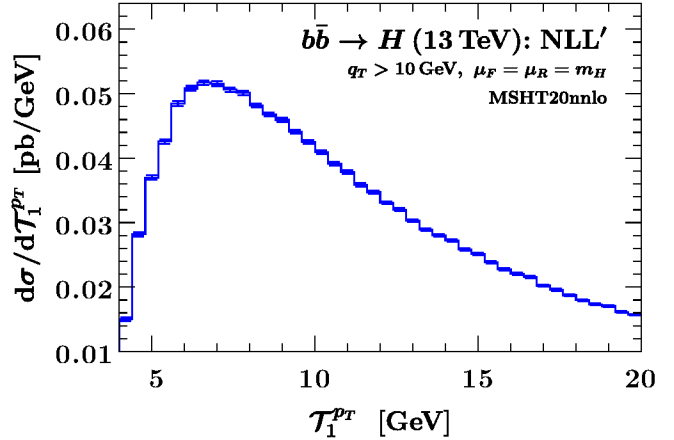FIG. 3: Nonsingular $\mathcal{T}_1^{p_T}$ spectrum for $b\bar{b} \to H$.

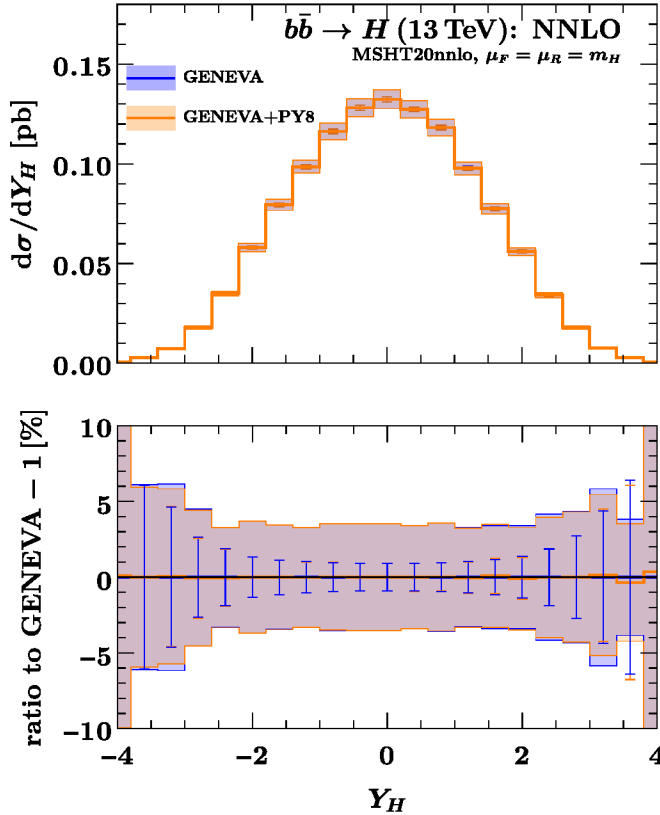FIG. 4: Resummed $\mathcal{T}_1^{p_T}$ spectrum for $b\bar{b} \to H$.

FIG. 5: Higgs boson rapidity spectrum in $b\bar{b} \to H$.
Results are shown at parton level and after showering.

improved subtraction techniques in GENEVA, which combine the projection-to-Born method with slicing to allow very small values of $r^{\rm cut}$ to be reached while correctly accounting for fiducial power corrections [71].

In fig. 1 we validate our predictions for the NNLO Higgs boson rapidity spectrum against an independent calculation from MCFM, obtained using zero-jettiness slicing [72, 73]. Note that compatibility with MCFM requires us to set in this case (and in this case alone) $\mu_F = m_H/4$, $\mu_R = m_H$ and to use the CT14NNLO PDF set [74]. We observe excellent agreement between the two calculations, both for the central value and for the 7-point scale variation bands.

B.   Resummed validation

The GENEVA method relies on an additive matching procedure of resummed and fixed-order calculations. It should therefore be the case that predictions for the 0−jet resolution variable (in this case, q_T) from the event generator are exactly N^{3}LL accurate by construction, at least at parton level. In fig. 2 we confirm this explicitly by comparison with a separate run of SCETLIB. We observe complete agreement for both central value and uncertainty bands, thus corroborating the correctness of our implementation.

C.   The 1/2−jet bin separation

A novel feature of this work is the use of $\mathcal{T}_1^{p_T}$ as a resolution variable to separate the 1− and 2−jet bins. We remind the reader that, in addition to the resummation of this variable at NLL′, the implementation of this variable in the event generator has required us to develop appropriate mappings for the splitting functions which spread the resummation over the higher multiplic-
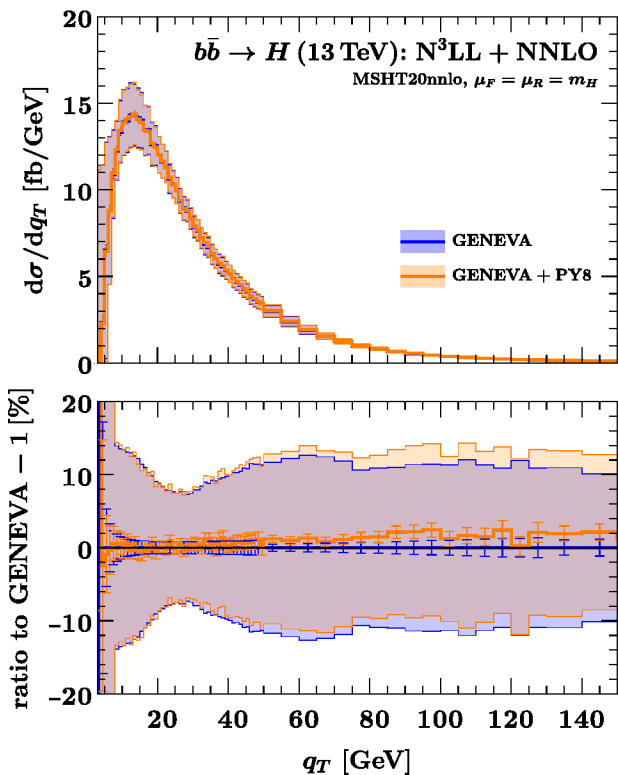
cision of the calculation ($\sim 0.2\%$). In the following we therefore will use $q_T^{\rm cut} = 1$ GeV as our default choice. We also remark that, as in several previous implementations of GENEVA for colour singlet production [21, 24, 27], we do not need to employ a reweighting procedure to account for missing nonsingular terms below $r^{\rm cut}$. This need has in any case been recently obviated by the development of

FIG. 6: Higgs boson q_T spectrum in $b\bar{b} \to H$.
Results are shown at parton level and after
showering.

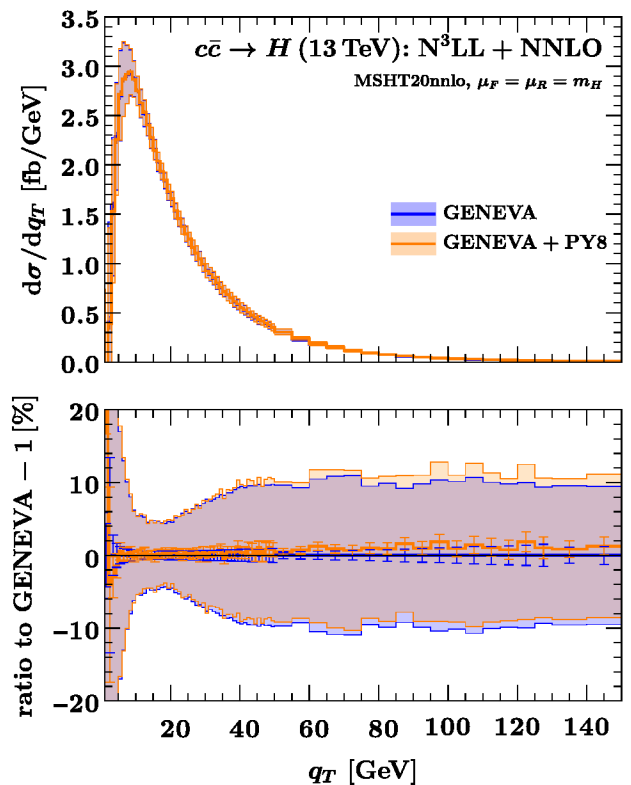FIG. 7: As in fig.6, but for $c\bar{c} \to H$.

ity phase space. Both issues are detailed in sec. IV.

In fig. 3 we verify that our implementation of eq. (21) does indeed have the correct logarithmic structure in the $\mathcal{T}_1^{p_T} \to 0$ limit. We plot the nonsingular difference between the leading power expansion of the factorisation formula and an exact fixed-order calculation at NLO_1 accuracy (where the subscript indicates the number of final state partons). We observe that the double logarithmic plot correctly shows a linear suppression of the nonsingular remnant, which approaches zero with falling $\mathcal{T}_1^{p_T}$. Fig. 4 shows the resummed $\mathcal{T}_1^{p_T}$ distribution at NLL' accuracy (for $q_T > 10$ GeV), which exhibits the characteristic Sudakov peak. In the following, we will set the value of $(\mathcal{T}_1^{p_T})^{\mathrm{cut}}$ appearing in the 1- and 2-jet GENEVA differential cross sections of eqs. (6) and (7) to 1 GeV, and the jet radius R appearing in eq. (15) to 0.4.

D. Effect of showering

One of the advantages of using $\mathcal{T}_1^{p_T}$ instead of $\mathcal{T}_1$ as 1-jet resolution variable is that it facilitates the matching to showers ordered in transverse momentum. In this work, we shower the partonic events with the p_T-ordered PYTHIA8 shower [75], setting the option `SpaceShower:dipoleRecoil=on`. This option ensures that the recoil momentum of ISR emissions is distributed within the colour dipole whenever kinematically possible (for FSR emissions, this is the default behaviour), thus reducing the impact of the shower on the colour singlet momentum.

In fig. 5, we show the effect of showering on the sole inclusive and differential quantity for $b\bar{b} \to H$, i.e. the Higgs boson rapidity. We observe that, as expected, the shower does not alter the distribution.

Moving to more exclusive quantities, in figs.6 and 7 we show the Higgs boson q_T spectrum in $b\bar{b} \to H$ and $c\bar{c} \to H$ respectively, again comparing parton-level predictions with those after showering. We observe extremely good agreement between our partonic results (which are formally $\mathrm{N}^3\mathrm{LL}+\mathrm{NNLO}$ accurate) and our showered results – indeed, the two distributions coincide exactly to within Monte Carlo error. While we cannot argue formally that this constitutes $\mathrm{N}^3\mathrm{LL}+\mathrm{NNLO}$ accuracy for this distribution after showering, the fact remains that the results are for all intents and purposes indistinguishable.

In figs.8 and 9, we show the rapidity and transverse momentum of the hardest jet in $b\bar{b} \to H$ respectively. The hardest jet is defined as the jet with the largest transverse momentum among the jets with transverse momentum larger than 30 GeV obtained clustering the final-state partons with an anti-k_T jet algorithm with jet radius $R = 0.4$. The effect of showering on these exclusive distributions is greater, reaching up to $\sim 15\%$ on the
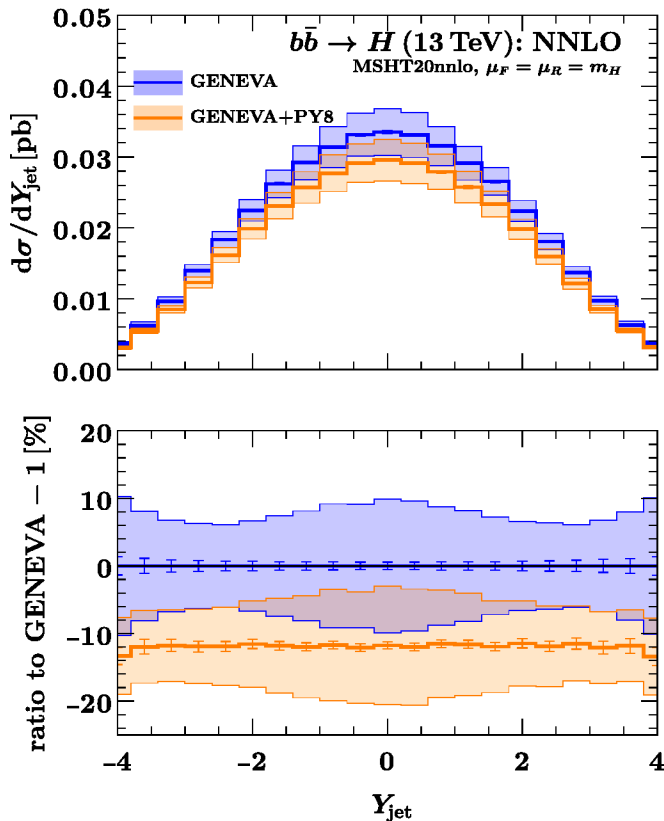
FIG. 8: Hardest jet rapidity spectrum in $b\bar{b} \to H$. Results are shown at parton level and after showering.

FIG. 9: Hardest jet p_T spectrum in $b\bar{b} \to H$. Results are shown at parton level and after showering.

central value.

VI. CONCLUSIONS

In this work we have investigated the use of transverse resolution variables to achieve NNLO+PS matching within the GENEVA framework. In particular, we combine q_T resummation at N^{3}LL, obtained via an interface to the SCETLIB library, with $\mathcal{T}_1^{p_T}$ resummation at NLL′. This combination of variables facilitates matching to transverse momentum ordered showers while also providing high accuracy predictions for the colour singlet transverse momentum. We have tested our framework on Higgs boson production in heavy-quark annihilation, in particular examining the $b\bar{b} \to H$ channel, finding good agreement with independent fixed order calculations and verifying that the resummed accuracy of the q_T distribution is preserved after showering to within the Monte Carlo error of the calculation.

In the future, the methods developed here could be extended to the production of other colour singlet processes. This could for example be useful in the context of M_W extractions – for example, in ref. [76], differential distributions for W and Z boson production obtained using the MiNNLOPS generator [6] are reweighted to N^{3}LL+NNLO accuracy with SCETLIB. Extending the
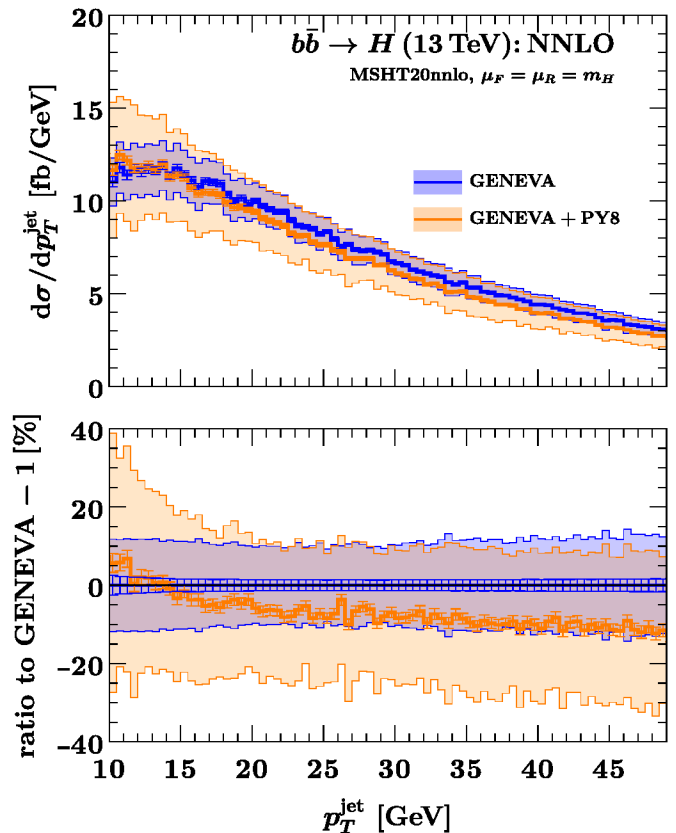
generators we have developed here to the Drell-Yan case would remove the need for this reweighting step, since we interface SCETLIB directly and reach N^{3}LL+NNLO accuracy in the q_T distribution by construction.

Another interesting direction to pursue is the extension of the resummation accuracy in $\mathcal{T}_1^{p_T}$ to NNLL′. This would allow matching fixed-order calculations for colour singlet production in association with a hard jet to parton shower algorithms. Although at present the most promising route to this goal seems to be using the normal, invariant mass definition of the one-jettiness (and indeed, both the required fixed-order and resummed calculations for the $Z + j$ process are now implemented in GENEVA [71, 77]), as in the colour singlet case the transverse nature of $\mathcal{T}_1^{p_T}$ is likely to facilitate matching to transverse momentum-ordered showers. Extension of the resummation accuracy would require the computation of an appropriate 2-loop soft function, which could for example be achieved using SOFTSERVE [78–80].

Finally, an important topic in perturbative calculations is the consistent estimation of theoretical uncertainties related to missing higher orders. Approaches based on theory nuisance parameters (TNPs) have shown promise in both resummed and fixed order calculations [81, 82] and how similar techniques could be applied to the event generation case is an interesting open

question. The fact that a direct application of the TNP approach to the resummed q_T spectrum has already been presented in ref. [81] perhaps suggests that generators of the kind we have presented in this work (using SCET-based resummation and q_T as resolution variable) may provide a starting point. We leave this to future work.

Appendix A: Profile scales and scale variation

The canonical boundary scales in b_T space are given by

virtuality: $\quad \mu_H = m_H, \quad \mu_B = b_0/b_T, \quad \mu_S = b_0/b_T,$
$$\mu_f = b_0/b_T, \quad \mu_0 = b_0/b_T,$$
rapidity: $\quad\quad\quad\quad \nu_B = m_H, \quad\quad \nu_S = b_0/b_T,$
$$\tag{A1}$$

where $b_0 \equiv 2e^{-\gamma_E} \approx 1.12291$, μ_H, (μ_B, ν_B), and (μ_S, ν_S) are the boundary scales for the hard, beam, and soft functions, and μ_f is the scale at which the PDFs inside the beam functions are evaluated. The rapidity anomalous dimension must also be resummed and μ_0 is its associated boundary scale. Evolution of each of the functions in eq. (11) from these scales to common scales μ, ν resums all canonical b_T-space logarithms $\ln^n[(b_0/b_T)/m_H]$. The corresponding resummed result in q_T space is then obtained via inverse Fourier transform.

Choosing scales which are functions of the variable being resummed facilitates deactivation of the resummation in the fixed-order region of phase space. We choose hybrid profile scales, depending on both b_T and q_T, as

$$\mu_H = \nu_B = \mu_{\rm FO} = m_H,$$
$$\mu_X = m_H\, f_{\rm run}\Big[\frac{q_T}{m_H}, \frac{1}{m_H}\mu_*\Big(\frac{b_0}{b_T}, \mu_X^{\rm min}\Big)\Big],$$
$$\mu_0 = \mu_*\Big(\frac{b_0}{b_T}, \mu_0^{\rm min}\Big), \tag{A2}$$

where $\mu_X \in \{\mu_B, \mu_S, \nu_S, \mu_f\}$. The function μ_* specifies our nonperturbative prescription, which prevents the beam and soft scales reaching values $1/b_T \lesssim \Lambda_{\rm QCD}$ and allows the inverse Fourier transform to q_T space to be performed. It is given by

$$\mu_*(x, y) = \sqrt{x^2 + y^2} \tag{A3}$$

$f_{\rm run}$ is the hybrid profile function given by [57]

$$f_{\rm run}(x, y) = 1 + g_{\rm run}(x)(y - 1), \tag{A4}$$

where $g_{\rm run}(x)$ determines the transition as a function of $x = q_T/m_H$,

$$g_{\rm run}(x) = \begin{cases} 1 & 0 < x \le x_1, \\ 1 - \frac{(x-x_1)^2}{(x_2-x_1)(x_3-x_1)} & x_1 < x \le x_2, \\ \frac{(x-x_3)^2}{(x_3-x_1)(x_3-x_2)} & x_2 < x \le x_3, \\ 0 & x_3 \le x, \end{cases} \tag{A5}$$

with transition points x_i for $i \in \{1, 2, 3\}$. The parameters x_1 and x_3 determine the start and end of the transition and $x_2 = (x_1 + x_3)/2$ corresponds to the turning point. We use $[x_1, x_2, x_3] = [0.1, 0.45, 0.8]$ as our central values.

The profile scales are varied as follows:

$$\mu_H = \mu_{\rm FO} = 2^{w_{\rm FO}}\, m_H,$$
$$\nu_B = \mu_{\rm FO}\, f_{\rm vary}^{v_{\nu_B}}\Big(\frac{q_T}{m_H}\Big),$$
$$\mu_X = \mu_{\rm FO}\, f_{\rm vary}^{v_{\mu_X}}\Big(\frac{q_T}{m_H}\Big) f_{\rm run}\Big[\frac{q_T}{m_H}, \frac{1}{m_H}\mu_*\Big(\frac{b_0}{b_T}, \frac{\mu_X^{\rm min}}{2^{w_{\rm FO}} f_{\rm vary}^{v_{\mu_X}}}\Big)\Big],$$
$$\text{for} \quad \mu_X \in \{\mu_B, \mu_S, \nu_S\},$$
$$\mu_f = 2^{w_F}\, m_H\, f_{\rm run}\Big[\frac{q_T}{m_H}, \frac{1}{m_H}\mu_*\Big(\frac{b_0}{b_T}, \frac{\mu_f^{\rm min}}{2^{w_F}}\Big)\Big],$$
$$\mu_0 = \mu_*\Big(\frac{b_0}{b_T}, \mu_0^{\rm min}\Big). \tag{A6}$$

Resummation uncertainties are gauged by varying the exponents v_{μ_B}, v_{ν_B}, v_{μ_S}, and v_{ν_S} about their central values $v_i = 0$ by ± 1. The function

$$f_{\rm vary}(x) = \begin{cases} 2(1 - x^2/x_3^2) & 0 \le x \le x_3/2, \\ 1 - 2(1 - x/x_3)^2 & x_3/2 < x \le x_3, \\ 1 & x_3 \le x, \end{cases} \tag{A7}$$

with $x \equiv q_T/m_H$ controls the size of the variations, ranging from a factor of 2 for $x = 0$ to 1 for $x \ge x_3$. Note that both the resummation itself and the associated resummation uncertainty is deactivated for $q_T \ge x_3 m_H$. The combined resummation uncertainty $\Delta_{\rm res}$ is calculated by enveloping 36 variations of suitable combinations of the v_i. For details, we refer the reader to ref. [53].

For the fixed-order uncertainty $\Delta_{\rm FO}$, we vary $\mu_{\rm FO}$ by a factor of 2 by taking $w_{\rm FO} = \{-1, 0, +1\}$ everywhere. A separate uncertainty Δ_{μ_f} is related to the DGLAP running of the PDFs, for which we vary the PDF scale μ_f by taking $w_F = \{-1, 0, +1\}$. In the nonsingular and fixed-order cross sections, this corresponds to taking $\mu_f \equiv \mu_F = 2^{w_F} m_H$. The resulting $\Delta_{\rm FO}$ and Δ_{μ_f}

are then given by the maximum envelope of the respective variations. Finally, a matching uncertainty Δ_{match} is obtained by varying x_2 in the range [0.2,0.6].

The total perturbative uncertainty for exclusive quantities is obtained by quadrature sum of the individual contributions, viz.

$$\Delta_{\text{total}}^2 = \Delta_{\text{FO}}^2 + \Delta_{\text{res}}^2 + \Delta_{\mu_f}^2 + \Delta_{\text{match}}^2. \qquad \text{(A8)}$$

For inclusive quantities, we instead take the conventional 7-point scale variation band.

Appendix B: Plus distributions

Following ref. [55], we define plus distributions of dimensionless arguments as

$$\mathcal{L}_n(x) \equiv \left[\frac{\Theta(x) \ln^n x}{x} \right]_+$$
$$= \lim_{\beta \to 0} \left[\frac{\Theta(x - \beta) \ln^n x}{x} + \delta(x - \beta) \frac{\ln^{n+1} \beta}{n + 1} \right], \qquad \text{(B1)}$$

$$\mathcal{L}^a(x) \equiv \left[\frac{\Theta(x)}{x^{1-a}} \right]_+$$
$$= \lim_{\beta \to 0} \left[\frac{\Theta(x - \beta)}{x^{1-a}} + \delta(x - \beta) \frac{x^a - 1}{a} \right]. \qquad \text{(B2)}$$

Solutions to the evolution equations for $\mathcal{T}_1^{p_T}$ are conveniently expressed in terms of the function $\mathcal{V}_a(x)$, which is defined as

$$\mathcal{V}_a(x) \equiv \frac{e^{-\gamma_E a}}{\Gamma(1 + a)} \left[a \mathcal{L}^a(x) + \delta(x) \right],$$

$$\mathcal{V}_a(k, \mu) \equiv \frac{1}{\mu} \mathcal{V}_a\left(\frac{k}{\mu} \right). \qquad \text{(B3)}$$

The $\mathcal{V}_a$ satisfy a number of useful identities,

$$\int dk' \mathcal{V}_a(k', \mu) \mathcal{V}_b(k - k', \mu) = \mathcal{V}_{a+b}(k, \mu), \qquad \text{(B4)}$$

$$\mathcal{V}_a(k, \mu) = \left(\frac{\mu'}{\mu} \right)^a \mathcal{V}_a(k, \mu'), \qquad \text{(B5)}$$

$$\mu \frac{d}{d\mu} \mathcal{V}_a(k, \mu) = -a \mathcal{V}_a(k, \mu). \qquad \text{(B6)}$$

Appendix C: One-loop expressions for $\mathcal{T}_1^{p_T}$ soft, beam and jet functions

Each of the soft, beam and jet functions admits a perturbative expansion in α_s of the form

$$F = \sum_{n=0}^{\infty} \left(\frac{\alpha_s}{4\pi} \right)^n F^{(n)} \qquad \text{(C1)}$$
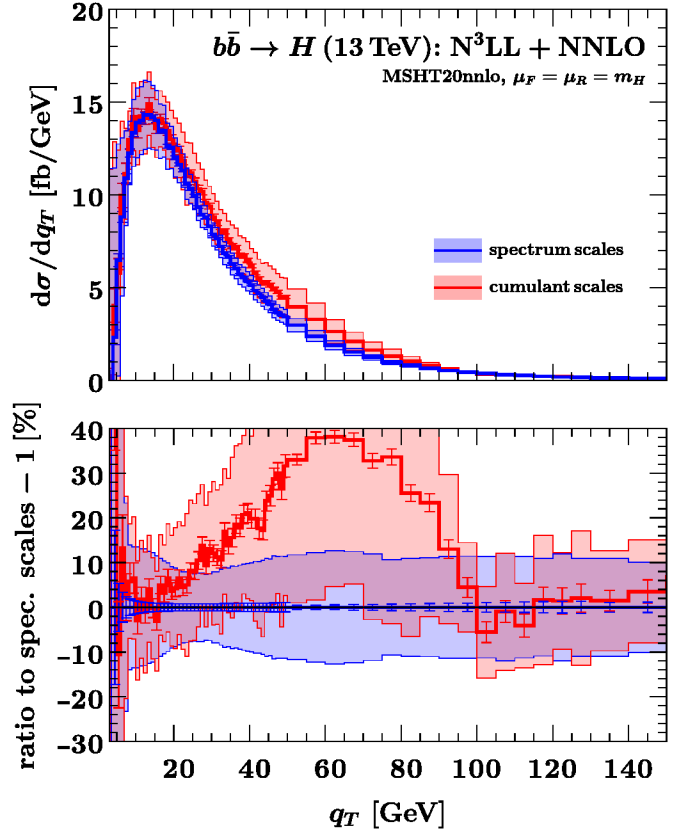

FIG. 10: Parton-level Higgs boson q_T spectrum in $b\bar{b} \to H$ for spectrum and cumulant scale settings.

for $F \in \{S, B, J\}$. Furthermore, the beam function can be written as a convolution between the normal parton distribution functions and perturbative kernels as

$$B_i\left(k, x, \mu, \frac{\nu}{\omega} \right) = \sum_m \int_x^1 \frac{dz}{z} \mathcal{I}_{im}\left(k, z, \mu, \frac{\nu}{\omega} \right) f_m\left(\frac{x}{z}, \mu \right) \qquad \text{(C2)}$$

where it is the kernels $\mathcal{I}$ that possess an expansion in α_s.

The one-loop expressions necessary for the $\mathcal{T}_1^{p_T}$ beam function at NLL' are given by

$$\mathcal{I}_{im}^{(1)}(z) = \delta_{im} \delta(1 - z) L_B^\mu \left(2 C_i \Gamma_0 L_B^\nu + \gamma_{\mu, B}^{i(0)} \right)$$
$$- 2 L_B^\mu P_{im}^{(0)}(z) + I_{im}^{(1)}(z), \qquad \text{(C3)}$$

$$I_{gq}^{(1)}(z) = z, \qquad \text{(C4)}$$

$$I_{qq}^{(1)}(z) = 1 - z, \qquad \text{(C5)}$$

$$I_{qg}^{(1)}(z) = 2z(1 - z), \qquad \text{(C6)}$$

where the logarithms are defined as

$$L_B^\mu = \ln \frac{\mu}{k}, \qquad L_B^\nu = \ln \frac{\nu}{\omega}. \qquad \text{(C7)}$$

The quark and gluon jet functions at one loop are given

by

$$J_q^{(1)}(k,\mu,\nu) = C_F \left[\left(7 - \frac{2\pi^2}{3} - 6\log 2 \right) \delta(k) \right.$$
$$\left. + \left(6 + 8\log\frac{\nu}{Q} \right) \mathcal{L}_0 \left(k, \frac{\mu}{Q} \right) \right] \quad \text{(C8)}$$

and

$$J_g^{(1)}(k,\mu,\nu) = \left[C_A \left(\frac{25}{12} - \frac{2\pi^2}{3} \right) + \beta_0 \left(\frac{17}{12} + 2\log 2 \right) \right] \delta(k)$$
$$+ \left[2\beta_0 + 8C_A\log\frac{\nu}{Q} \right] \mathcal{L}_0 \left(k, \frac{\mu}{Q} \right) . \quad \text{(C9)}$$

The soft function at one-loop order was calculated in ref. [61]. While the full expression is rather lengthy (and can be found in that reference after setting $\beta = \gamma = 1$), the term proportional to $\delta(k_S)$ is given by

$$s_\kappa^{(1)} = -(C_a + C_b + C_J) \frac{\pi^2}{6}$$
$$- 2C_J \log^2 R_J \left[2 + \Theta(R_J - 1) \right] \quad \text{(C10)}$$

where we have neglected power-suppressed terms in R_J^2. These have been shown to have at worst a moderate numerical impact, even for values of the jet radius R_J up to 1.5 [61].

Appendix D: Effect of scale setting choices on the q_T spectrum

In fig.10 we show the Higgs boson q_T spectrum in $b\bar{b} \to H$ for spectrum (blue) and cumulant (red) scale settings. These different scale choices were discussed in detail in sec. V A. We observe that both spectra are in good agreement in the peak and the tail region. In particular for the tail of distribution, this behaviour is expected as both distributions are matched to the same fixed-order prediction and therefore must agree in the fixed-order limit. In the transition region, however, the higher order terms have a significant effect which can be as large as 40%. The large size of this effect is peculiar to the $b\bar{b} \to H$ process, and its origin is discussed in detail in ref. [33].

Appendix E: Flavour structure of Geneva

The GENEVA method is sufficiently general that a number of different choices for the resolution variables r_0 and r_1 may be made, each resulting in an NNLO+PS accurate generator. To date, choices for r_0 include the transverse momentum of the colour singlet q_T, the $0-$jettiness $\mathcal{T}_0$ and the hardest jet transverse momentum $p_{1,T}^j$, while choices for r_1 include the conventional $1-$jettiness $\mathcal{T}_1$, the second jet transverse momentum $p_{2,T}^j$ and, as of this work, the $1-$jettiness with transverse momentum measures $\mathcal{T}_1^{p_T}$. It is clear that the number of different permutations now available may cause confusion when one wishes to refer to a specific implementation of GENEVA. Inspired by the origins of the term 'flavour' in particle physics (due to Gell-Mann), we therefore propose a nomenclature which should serve to clarify exactly which choice of resolution variables has been made in a given case. This appears in tab. II.

Flavour	r_0	r_1	Reference
Vanilla (V)	$\mathcal{T}_0$	$\mathcal{T}_1$	[13]
Raspberry ripple (RR)	q_T	$\mathcal{T}_1$	[24]
Tutti frutti (TF)	$p_{1,T}^j$	$p_{2,T}^j$	[27]
Mint choc chip (MCC)	q_T	$\mathcal{T}_1^{p_T}$	This work

TABLE II: Flavours of GENEVA implementation.

[1] G. Billis, B. Dehnadi, M. A. Ebert, J. K. L. Michel, and F. J. Tackmann, Phys. Rev. Lett. **127**, 072001 (2021), arXiv:2102.08039 [hep-ph].
[2] X. Chen, T. Gehrmann, E. W. N. Glover, A. Huss, B. Mistlberger, and A. Pelloni, Phys. Rev. Lett. **127**, 072002 (2021), arXiv:2102.07607 [hep-ph].
[3] X. Chen, T. Gehrmann, E. W. N. Glover, A. Huss, P. F. Monni, E. Re, L. Rottoli, and P. Torrielli, Phys. Rev. Lett. **128**, 252001 (2022), arXiv:2203.01565 [hep-ph].
[4] X. Chen, P. Jakubčík, M. Marcoli, and G. Stagnitto, (2025), arXiv:2505.10618 [hep-ph].
[5] S. Alioli, C. W. Bauer, C. Berggren, A. Hornig, F. J. Tackmann, *et al.*, JHEP **1309**, 120 (2013), arXiv:1211.7049 [hep-ph].
[6] P. F. Monni, P. Nason, E. Re, M. Wiesemann, and G. Zanderighi, JHEP **05**, 143 (2020), arXiv:1908.06987 [hep-ph].
[7] J. M. Campbell, S. Höche, H. T. Li, C. T. Preuss, and P. Skands, Phys. Lett. B **836**, 137614 (2023), arXiv:2108.07133 [hep-ph].
[8] B. K. El-Menoufi, C. T. Preuss, L. Scyboz, and P. Skands, (2024), arXiv:2412.14242 [hep-ph].
[9] M. Dasgupta, F. A. Dreyer, K. Hamilton, P. F. Monni, G. P. Salam, and G. Soyez, Phys. Rev. Lett. **125**, 052002 (2020), arXiv:2002.11114 [hep-ph].
[10] M. van Beekveld *et al.*, (2024), arXiv:2406.02661 [hep-ph].
[11] F. Herren, S. Höche, F. Krauss, D. Reichelt, and M. Schoenherr, JHEP **10**, 091 (2023), arXiv:2208.06057 [hep-ph].
[12] S. Höche, F. Krauss, and D. Reichelt, (2024), arXiv:2404.14360 [hep-ph].

[13] S. Alioli, C. W. Bauer, C. Berggren, F. J. Tackmann, and J. R. Walsh, Phys. Rev. **D92**, 094020 (2015), arXiv:1508.01475 [hep-ph].

[14] I. W. Stewart, F. J. Tackmann, and W. J. Waalewijn, Phys. Rev. Lett. **105**, 092002 (2010), arXiv:1004.2489 [hep-ph].

[15] S. Alioli, A. Broggio, S. Kallweit, M. A. Lim, and L. Rottoli, Phys. Rev. D **100**, 096016 (2019), arXiv:1909.02026 [hep-ph].

[16] S. Alioli, A. Broggio, A. Gavardi, S. Kallweit, M. A. Lim, R. Nagar, D. Napoletano, and L. Rottoli, JHEP **04**, 254 (2021), arXiv:2009.13533 [hep-ph].

[17] S. Alioli, A. Broggio, A. Gavardi, S. Kallweit, M. A. Lim, R. Nagar, D. Napoletano, and L. Rottoli, JHEP **04**, 041 (2021), arXiv:2010.10498 [hep-ph].

[18] S. Alioli, A. Broggio, A. Gavardi, S. Kallweit, M. A. Lim, R. Nagar, and D. Napoletano, Phys. Lett. B **818**, 136380 (2021), arXiv:2103.01214 [hep-ph].

[19] T. Cridge, M. A. Lim, and R. Nagar, Phys. Lett. B **826**, 136918 (2022), arXiv:2105.13214 [hep-ph].

[20] S. Alioli, G. Billis, A. Broggio, A. Gavardi, S. Kallweit, M. A. Lim, G. Marinelli, R. Nagar, and D. Napoletano, JHEP **06**, 205 (2023), arXiv:2212.10489 [hep-ph].

[21] S. Alioli, G. Billis, A. Broggio, A. Gavardi, S. Kallweit, M. A. Lim, G. Marinelli, R. Nagar, and D. Napoletano, JHEP **05**, 128 (2023), arXiv:2301.11875 [hep-ph].

[22] I. W. Stewart, F. J. Tackmann, and W. J. Waalewijn, Phys. Rev. D **81**, 094035 (2010), arXiv:0910.0467 [hep-ph].

[23] S. Alioli, A. Broggio, and M. A. Lim, JHEP **01**, 066 (2022), arXiv:2111.03632 [hep-ph].

[24] S. Alioli, C. W. Bauer, A. Broggio, A. Gavardi, S. Kallweit, M. A. Lim, R. Nagar, D. Napoletano, and L. Rottoli, Phys. Rev. D **104**, 094020 (2021), arXiv:2102.08390 [hep-ph].

[25] P. F. Monni, E. Re, and P. Torrielli, Phys. Rev. Lett. **116**, 242001 (2016), arXiv:1604.02191 [hep-ph].

[26] W. Bizon, P. F. Monni, E. Re, L. Rottoli, and P. Torrielli, JHEP **02**, 108 (2018), arXiv:1705.09127 [hep-ph].

[27] A. Gavardi, M. A. Lim, S. Alioli, and F. J. Tackmann, JHEP **12**, 069 (2023), arXiv:2308.11577 [hep-ph].

[28] I. W. Stewart, F. J. Tackmann, J. R. Walsh, and S. Zuberi, Phys. Rev. D **89**, 054001 (2014), arXiv:1307.1808.

[29] P. Cal, M. A. Lim, D. J. Scott, F. J. Tackmann, and W. J. Waalewijn, JHEP **03**, 155 (2025), arXiv:2408.13301 [hep-ph].

[30] P. Nason, JHEP **11**, 040 (2004), hep-ph/0409146.

[31] M. A. Ebert, J. K. L. Michel, F. J. Tackmann, *et al.*, DESY-17-099 (2018), webpage: http://scetlib.desy.de.

[32] L. Buonocore, M. Grazzini, J. Haag, L. Rottoli, and C. Savoini, Phys. Rev. D **106**, 014008 (2022), arXiv:2201.11519 [hep-ph].

[33] P. Cal, R. von Kuk, M. A. Lim, and F. J. Tackmann, Phys. Rev. D **110**, 076005 (2024), arXiv:2306.16458 [hep-ph].

[34] C. Biello, A. Sankar, M. Wiesemann, and G. Zanderighi, Eur. Phys. J. C **84**, 479 (2024), arXiv:2402.04025 [hep-ph].

[35] F. Bishara, U. Haisch, P. F. Monni, and E. Re, Phys. Rev. Lett. **118**, 121801 (2017), arXiv:1606.09253 [hep-ph].

[36] J. C. Collins and D. E. Soper, Nucl. Phys. B **193**, 381 (1981), [Erratum: Nucl.Phys.B 213, 545 (1983)].

[37] J. C. Collins and D. E. Soper, Nucl. Phys. B **197**, 446 (1982).

[38] J. C. Collins, D. E. Soper, and G. F. Sterman, Nucl. Phys. B **250**, 199 (1985).

[39] S. Catani, D. de Florian, and M. Grazzini, Nucl. Phys. B **596**, 299 (2001), arXiv:hep-ph/0008184.

[40] D. de Florian and M. Grazzini, Nucl. Phys. B **616**, 247 (2001), arXiv:hep-ph/0108273.

[41] J. Collins, *Foundations of perturbative QCD*, Vol. 32 (Cambridge University Press, 2013).

[42] C. W. Bauer, S. Fleming, and M. E. Luke, Phys. Rev. D **63**, 014006 (2000), hep-ph/0005275.

[43] C. W. Bauer, S. Fleming, D. Pirjol, and I. W. Stewart, Phys. Rev. D **63**, 114020 (2001), hep-ph/0011336.

[44] C. W. Bauer and I. W. Stewart, Phys. Lett. B **516**, 134 (2001), hep-ph/0107001.

[45] C. W. Bauer, D. Pirjol, and I. W. Stewart, Phys. Rev. D **65**, 054022 (2002), hep-ph/0109045.

[46] C. W. Bauer, S. Fleming, D. Pirjol, I. Z. Rothstein, and I. W. Stewart, Phys. Rev. D **66**, 014017 (2002), hep-ph/0202088.

[47] T. Becher and M. Neubert, Eur. Phys. J. C **71**, 1665 (2011), arXiv:1007.4005 [hep-ph].

[48] M. G. Echevarria, A. Idilbi, and I. Scimemi, JHEP **07**, 002 (2012), arXiv:1111.4996 [hep-ph].

[49] J.-Y. Chiu, A. Jain, D. Neill, and I. Z. Rothstein, JHEP **05**, 084 (2012), arXiv:1202.0814 [hep-ph].

[50] Y. Li, D. Neill, and H. X. Zhu, Nucl. Phys. B **960**, 115193 (2020), arXiv:1604.00392 [hep-ph].

[51] J.-y. Chiu, A. Jain, D. Neill, and I. Z. Rothstein, Phys. Rev. Lett. **108**, 151601 (2012), arXiv:1104.0881 [hep-ph].

[52] M. A. Ebert and F. J. Tackmann, JHEP **02**, 110 (2017), arXiv:1611.08610 [hep-ph].

[53] M. A. Ebert, J. K. L. Michel, I. W. Stewart, and F. J. Tackmann, JHEP **04**, 102 (2021), arXiv:2006.11382 [hep-ph].

[54] G. Billis, F. J. Tackmann, and J. Talbert, JHEP **03**, 182 (2020), arXiv:1907.02971 [hep-ph].

[55] Z. Ligeti, I. W. Stewart, and F. J. Tackmann, Phys. Rev. D **78**, 114014 (2008), arXiv:0807.1926 [hep-ph].

[56] R. Abbate, M. Fickinger, A. H. Hoang, V. Mateu, and I. W. Stewart, Phys. Rev. D **83**, 074021 (2011), arXiv:1006.3080 [hep-ph].

[57] G. Lustermans, J. K. L. Michel, F. J. Tackmann, and W. J. Waalewijn, JHEP **03**, 124 (2019), arXiv:1901.03331 [hep-ph].

[58] G. Billis, J. K. L. Michel, and F. J. Tackmann, JHEP **02**, 170 (2025), arXiv:2411.16004 [hep-ph].

[59] A. J. Larkoski, D. Neill, and J. Thaler, JHEP **04**, 017 (2014), arXiv:1401.2158 [hep-ph].

[60] I. W. Stewart, F. J. Tackmann, J. Thaler, C. K. Vermilion, and T. F. Wilkason, JHEP **11**, 072 (2015), arXiv:1508.01516 [hep-ph].

[61] D. Bertolini, D. Kolodrubetz, D. Neill, P. Pietrulewicz, I. W. Stewart, F. J. Tackmann, and W. J. Waalewijn, JHEP **07**, 099 (2017), arXiv:1704.08262 [hep-ph].

[62] J. Thaler and K. Van Tilburg, JHEP **03**, 015 (2011), arXiv:1011.2268 [hep-ph].

[63] J. Thaler and K. Van Tilburg, JHEP **02**, 093 (2012), arXiv:1108.2701 [hep-ph].

[64] A. Banfi, G. P. Salam, and G. Zanderighi, JHEP **08**, 062 (2004), arXiv:hep-ph/0407287.

[65] T. Becher and M. Neubert, JHEP **07**, 108 (2012), arXiv:1205.3806 [hep-ph].

[66] T. Becher, M. Neubert, and L. Rothen, JHEP **10**, 125 (2013), arXiv:1307.0025 [hep-ph].

[67] A. Gavardi, *Next-to-next-to-leading order predictions for diboson production in hadronic scattering combined with parton showers*, Ph.D. thesis, Università degli Studi di Milano-Bicocca, Italy, Milan Bicocca U. (2023).

[68] S. Bailey, T. Cridge, L. A. Harland-Lang, A. D. Martin, and R. S. Thorne, Eur. Phys. J. C **81**, 341 (2021), arXiv:2012.04684 [hep-ph].

[69] R. L. Workman *et al.* (Particle Data Group), PTEP **2022**, 083C01 (2022).

[70] R. V. Harlander, S. Liebler, and H. Mantler, Comput. Phys. Commun. **184**, 1605 (2013), arXiv:1212.3249 [hep-ph].

[71] S. Alioli, G. Billis, A. Broggio, and G. Stagnitto, (2025), arXiv:2504.11357 [hep-ph].

[72] R. Boughezal, J. M. Campbell, R. K. Ellis, C. Focke, W. Giele, X. Liu, F. Petriello, and C. Williams, Eur. Phys. J. C **77**, 7 (2017), arXiv:1605.08011 [hep-ph].

[73] R. Mondini and C. Williams, JHEP **05**, 045 (2021), arXiv:2102.05487 [hep-ph].

[74] S. Dulat, T.-J. Hou, J. Gao, M. Guzzi, J. Huston, P. Nadolsky, J. Pumplin, C. Schmidt, D. Stump, and C. P. Yuan, Phys. Rev. D **93**, 033006 (2016), arXiv:1506.07443 [hep-ph].

[75] T. Sjöstrand, S. Mrenna, and P. Z. Skands, Comput. Phys. Commun. **178**, 852 (2008), arXiv:0710.3820 [hep-ph].

[76] V. Chekhovsky *et al.* (CMS), (2024), arXiv:2412.13872 [hep-ex].

[77] S. Alioli, G. Bell, G. Billis, A. Broggio, B. Dehnadi, M. A. Lim, G. Marinelli, R. Nagar, D. Napoletano, and R. Rahn, Phys. Rev. D **109**, 094009 (2024), arXiv:2312.06496 [hep-ph].

[78] G. Bell, R. Rahn, and J. Talbert, JHEP **07**, 101 (2019), arXiv:1812.08690 [hep-ph].

[79] G. Bell, R. Rahn, and J. Talbert, JHEP **09**, 015 (2020), arXiv:2004.08396 [hep-ph].

[80] G. Bell, B. Dehnadi, T. Mohrmann, and R. Rahn, (2023), arXiv:2312.11626 [hep-ph].

[81] F. J. Tackmann, (2024), arXiv:2411.18606 [hep-ph].

[82] M. A. Lim and R. Poncelet, (2024), arXiv:2412.14910 [hep-ph].